sciendo

DOI 10.2478/ama-2024-0013

acta mechanica et automatica, vol.18 no.1 (2024)

FRICTION FORCE REDUCTION EFFICIENCY IN SLIDING MOTION UNDER TANGENTIAL VIBRATIONS OF ELASTIC SUPPORT

Mariusz LEUS*, Paweł GUTOWSKI*

*Faculty of Mechanical Engineering and Mechatronics, West Pomeranian University of Technology in Szczecin, al. Piastów 19, 70-310 Szczecin, Poland

mariusz.leus@zut.edu.pl, pawel.gutowski@zut.edu.pl

received 18 May 2023, revised 6 July 2023, accepted 6 July 2023

Abstract: The efficiency of reducing the friction force in sliding motion under the influence of forced vibrations of an elastic substrate significantly depends on the direction of these vibrations in relation to the sliding direction. This article presents a comparison of computational models developed by the authors to estimate the friction force in sliding motion under longitudinal and transverse tangential vibrations of the substrate. Fundamental differences between these models are discussed, and the results of comparative analyses of the impact of tangential vibrations on the friction force depending on their direction are presented. In the developed models describing the friction force, dynamic friction models of Dahl and Dupont and the so-called LuGre model were utilised. The analyses were performed as a function of the sliding velocity and two basic parameters of vibration, which are frequency f and amplitude u0. It has been shown that under longitudinal vibrations, the key parameter, which determines the occurrence of friction force reduction at a given driving velocity vd, is the amplitude va of vibration velocity. However, the level of this reduction cannot be determined unequivocally based on the value of this parameter alone since the identical value va can be obtained at different magnitudes of the frequency and amplitude of vibrations, and the reduction level is a nonlinear function of these parameters. The results of simulation analyses were verified experimentally.

Key words: sliding motion, tangential vibrations, friction force reduction

1. INTRODUCTION

The phenomenon of friction force reduction in sliding motion was and still is a subject of interest to scientists around the world. This stems from its utilitarian significance. However, to date, this phenomenon has not been fully researched and described, and the published results of experimental tests and simulating analyses are usually patchy, address narrow ranges of variability of the analysed parameters and are often ambiguous and even contradictory.

This phenomenon is used in practice in many branches of modern industry. Its most important applications are found in the machine tool industry and the oil mining industry. In the machine tool industry, it is used to reduce the cutting force in all machining processes, including milling, turning, drilling and grinding [1–11]. In the oil drilling industry, it is used to reduce the friction force between the drill string and the borehole wall and to reduce the stick–slip motion [12–20].

The mechanism of friction resistance reduction depends on the direction of vibrations in relation to both the plane and the direction of sliding and is different under vibrations that are normal and those that are tangential to the plane of sliding. In the case of tangential vibrations, the mechanism of reduction is different under longitudinal vibrations – in the direction of sliding, and different under transverse vibrations – perpendicular to this direction.

It was demonstrated in previous studies [21, 22] utilising the so-called dynamic models of friction of Dahl [23, 24] and Dupont [25, 26] that in the case of longitudinal tangential vibrations, the reduction in frictional forces in sliding motion results from cyclical changes in the sign of the relative velocity vector of the contact surface of the moving body and the support occurring in each vibration cycle, whenever the amplitude of the velocity of these vibrations is greater than the sliding velocity. This does not need to be associated with the change in the sign of friction force vector, as it results according to the Coulomb model. In the case of transverse vibrations, the change in friction resistance is a consequence of changes in the direction of the friction force and its oscillations around the direction of sliding in macroscale, due to which this force decomposes into two components, only one of which operates along the direction of sliding, that is, in the direction of the driving force [27–30]. In the case of normal vibrations, the view prevails that the reduction in friction resistance in sliding motion in the presence of these vibrations results from the change in the average distance between contacting surfaces, which reduces the normal interactions between the body being moved and the support [31, 32, 33].

This paper presents the outline of computational models developed by the authors of [21, 22, 29], which are utilised in conducting simulation analyses of friction force reduction in sliding motion by imposing vibrations tangent to the sliding plane on the support along which the sliding motion is conducted. These mo-dels are based on dynamic equations of motion of the sliding body. To describe the friction force, the so-called dynamic friction models of Dahl, Dupont and LuGre, in which the compliance characteristics of the contact zone of the sliding body and of the support have been considered, are utilised. The developed models were used to conduct comparative analyses of the level of friction force reduction in longitudinal tangential vibrations and transverse

DOI 10.2478/ama-2024-0013

tangential vibrations. These analyses were performed as a function of two principal parameters of vibrations, namely, frequency and amplitude, and as a function of the drive velocity. The obtained results were compared with the results of experimental investigations.

2. COMPUTATIONAL MODELS

To describe changes in the friction force in sliding motion proceeding on the support subjected to forced vibrations, computational models developed by the authors and described in detail in [21, 22, 29] were utilised, in which the contact area of the body being moved and the vibrating support are modelled by a singular, deformable, spring-damping substitute element MN (Fig. 1), which incorporates the stiffness of the contact zone in the direction of sliding and its damping.

In these models, dynamic friction models were used to describe the friction force, whose magnitude is a function of the elastic deformation s of the contact measured in the sliding plane.

In the Dahl and Dupont models, the relationship between friction force $\mathrm{F_F}$ and elastic deformation s of the contact is described by the following relationship:

$$F_F = k_t s, \tag{1}$$

while in the LuGre model [34, 35] from the relationship:

$$F_F = k_t s + h_t \dot{s} + h_v v_r \tag{2}$$

where $\mathrm{k_t}$ is the contact stiffness coefficient in the tangential direction, $\mathrm{h_t}$ is the contact damping coefficient at tangential deformation, $\mathrm{k_v}$ is the viscous contact damping coefficient and $\mathrm{v_r}$ is the relative movement velocity of the body being moved and vibrating support.

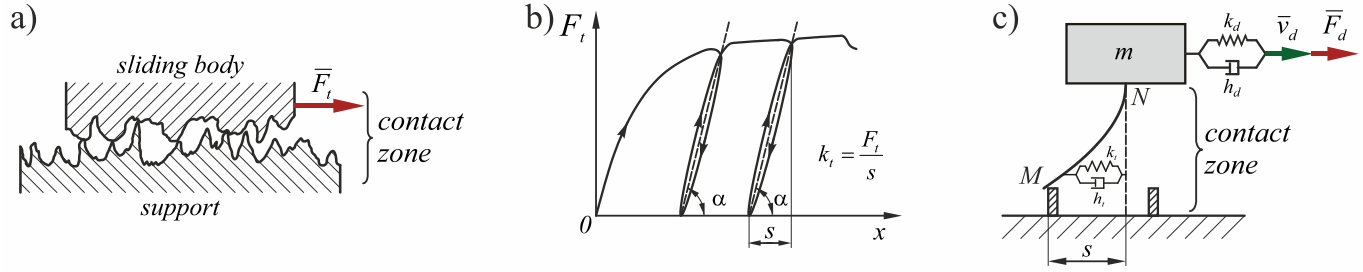

Fig. 1. Modelling of the contact zone in developed models: (a) the real contact, (b) shear compliance characteristic of the contact, (c) model of contact at sliding motion

The rate $\dot{s}$ of the increase in the contact elastic deformation in the Dahl and Dupont models is described by a general relationship in the following form:

$$\dot{s} = \frac{ds}{dt} = v_r \left[1 - \gamma(s, v_r) \frac{k_t s}{\mu F_N} sgn(v_r)\right]^{\kappa} \tag{3}$$

The magnitude of the function $\gamma(s, v_r)$ in the Dupont model depends on the magnitude of the elastic deformation s of the contact. Relevant relationships are provided in Refs [25, 26]. In the Dahl model, on the other hand, the value of this function is equal to 1. The method of selecting the exponent κ is provided in Ref [36]. In the developed models, $\kappa = 1$ was adopted.

In the LuGre model, the rate $\dot{s}$ of the elastic deformation increase is described by the following relationship:

$$\dot{s} = \frac{ds}{dt} = v_r - \frac{|v_r|}{g(v_r)} s \tag{4}$$

where

$$g(v_r) = \frac{1}{k_t}\left[F_C + (F_S - F_C) e^{-(v_r/v_S)^2}\right] \tag{5}$$

where F_C is the Coulomb friction force, $F_C = \mu F_N$, F_S is the static friction force and v_S is the Stribeck velocity.

In the LuGre model, it was assumed that in the absence of movement, the following relationship exists between the coefficient of tangential rigidity k_t of the contact and the damping coefficient h_t:

$$h_t = 2\sqrt{m k_t} \tag{6}$$

In the case of motion, the damping factor is also a function of relative velocity v_r and is described by the following relationship:

$$h_t(v_r) = h_t e^{-\left(\frac{v_r}{v_e}\right)^2} \tag{7}$$

Olson, in the calculation examples presented in Ref. [35], assumed that $v_e = v_S$.

In the developed models, it is assumed that the elastic deflection s of the contact at any moment can be presented as the effect of displacement of the ends *M* and *N* of the elastic element *MN* modelling this contact. It is measured in the plane of sliding (Fig. 2) and can be determined by the coordinates of points *M* and *N'*, where *N'* is the projection of point *N* on the plane of sliding.

In the case of longitudinal vibrations, the direction of this deformation may be opposite to, or in the same direction as, the sliding movement (Fig. 3). The change in the direction of elastic deformation of the contact is equivalent to the change in the sign of the friction force. However, this change does not occur with the turn of the vector $\vec{v}_r$ of relative motion velocity taking place when the amplitude of the vibration velocity v_a is greater than that of the slip velocity $\dot{x}$. At the m oment of change in the sign of the relative velocity vector $\vec{v}_r$ (Fig. 3), the initiation or termination of friction force reduction, in the case of longitudinal vibrations, occurs.

In the case of transverse vibrations, the direction of elastic deformation of the contact is variable over time and oscillates around the direction of the macroscopic movement of the shifted body. At an optional moment, it is defined by the angle $\beta = \beta(t)$. This direction is consistent with the direction of relative motion and direction of relative velocity $\vec{v}_r$ of the shifted body and vibrating support. The vector of the friction force F_F is in the same direction (Fig. 4).

DOI 10.2478/ama-2024-0013

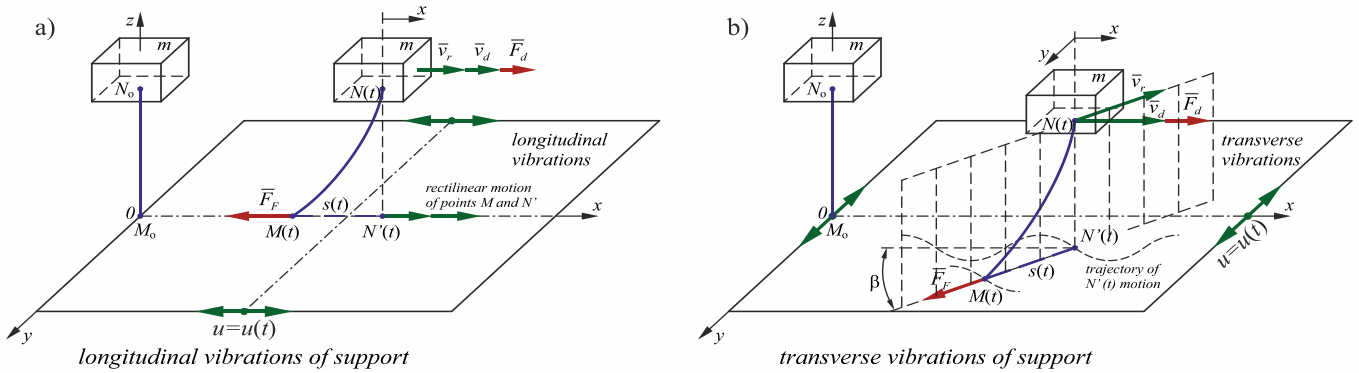

Fig. 2. Motion of a body and elastic deformation of the contact zone at tangential vibrations of the support: (a) longitudinal, (b) transverse vibrations

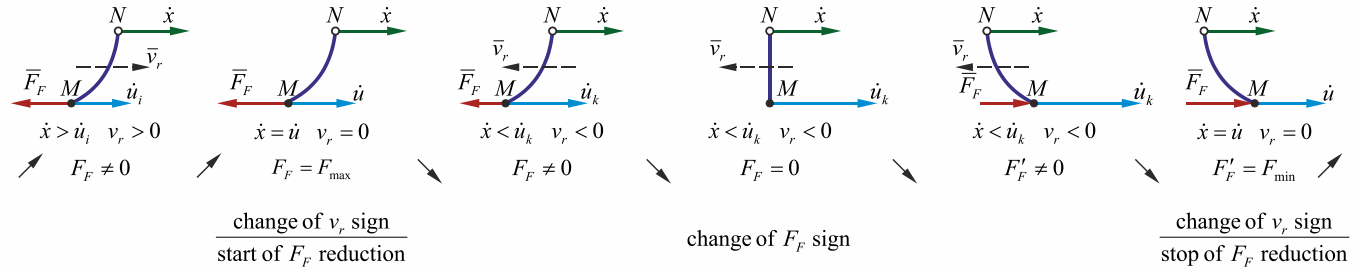

Fig. 3. Change in the value and sign of friction force vector $\vec{F}_F$ under longitudinal vibrations of the support

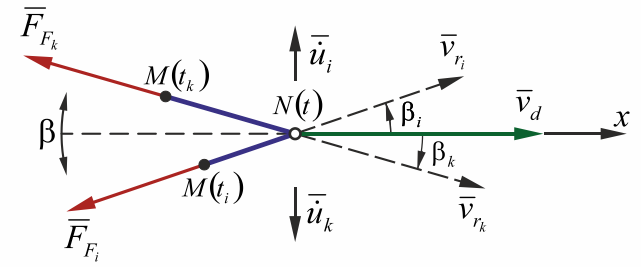

Fig. 4. Change in the direction of friction force vector $\vec{F}_F$ under transverse vibrations of the support

The movement of a shifted body on the vibrating support is described by the dynamic equations of motion. In the case of longitudinal vibrations, it is one equation in the following form:

$$m\ddot{x} = F_d - F_F, \tag{8}$$

while in the case of tangential transverse vibrations, these are the two following equations:

$$m\ddot{x} = F_d - F_F \cos\beta \tag{9}$$

$$m\ddot{y} = F_F \sin\beta \tag{10}$$

where F_d is the driving force, F_F is the friction force and m is the mass of the shifted body.

The average value $\tilde{F}_{Fx}$ of the friction force in the direction of driving force F_d (along the *0x* axis) during a single vibration period *T* corresponds to the value of the driving force necessary to set the body in sliding motion and to maintain this motion. Its value can be determined from the following relationship:

$$F_d = \tilde{F}_{F_x} = \frac{1}{n}\sum_{i=1}^{n} F_{F_x}(t + \Delta t) \tag{11}$$

where n is the number of time intervals to which a single vibration period *T* has been divided.

The aforementioned relationships were used in mathematical models for analysis of the influence of longitudinal tangential vibrations [21, 22] and transverse tangential vibrations [29] on the friction force in sliding motion, which were developed in the MATLAB/Simulink environment. After verification, these models were used in the simulating analyses.

3. SIMULATING ANALYSES

The condition for the occurrence of a reduction in the average friction force in the sliding movement during longitudinal tangential vibrations is a cyclic change in the sign of the relative velocity vector $\vec{v}_r$ of the substrate and shifted body in each vibration period. For this phenomenon to occur, the amplitude of vibration velocity v_a must be greater than that of the average sliding velocity, which is equal to the driving velocity v_d in this period. The following condition must therefore be met:

$$\psi = \frac{v_d}{v_a} < 1 \tag{12}$$

The influence of vibrations on the friction force in sliding motion can be illustrated in the form of graphs representing changes in the driving force F_d, whose average value corresponds to the average value $\tilde{F}_{F_x}$ of the friction force in the direction of sliding, as a function of the coefficient ψ, as defined earlier. The relationships presented in this way are, however, ambiguous because the driving force in sliding motion at the vibrating substrate is a nonlinear function of both the sliding velocity (driving velocity v_d) and amplitude v_a of vibration velocity. At the same magnitude of the parameter ψ, the friction force reduction level may be different, depending on the magnitude of v_a or v_d.

This problem is illustrated in Figs. 5 and 6, which present the profiles of normalised driving force F_d/F_C, that is, driving force F_d compared to Coulomb's friction force F_C, as a function of parame-

DOI 10.2478/ama-2024-0013

ter ψ for various predetermined sliding velocities v_d at varying amplitudes v_a of vibration velocity (Fig. 5) and analogous profiles at a fixed amplitude v_a but changing driving velocity v_d (Fig. 6). These diagrams were generated both under longitudinal and transverse tangential vibrations.

It is apparent from these profiles of F_d/F_C how different can be the level of the friction force reduction in the sliding motion at the same value of the parameter ψ, but at simultaneously different driving velocity v_d, or at the same value of ψ, but a different amplitude v_a of the vibration velocity.

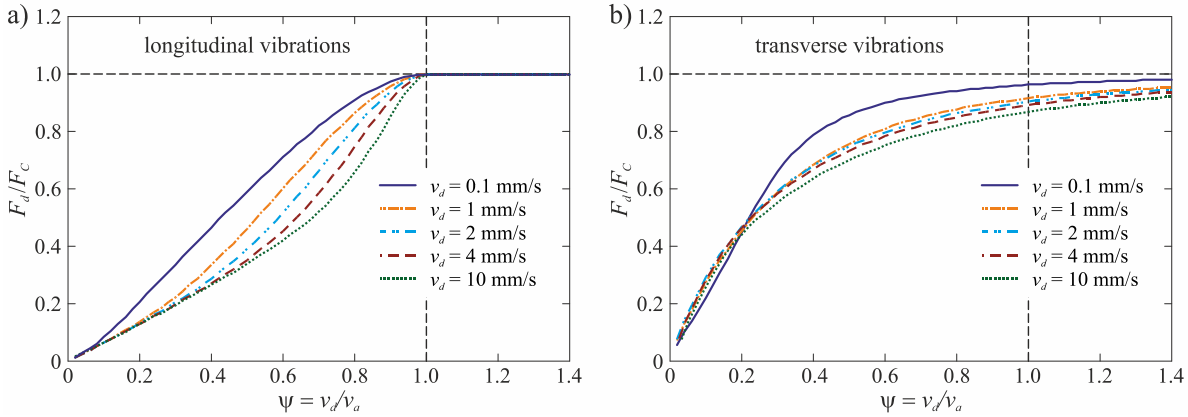

Fig. 5. Profiles of changes in F_d/F_C as a function of parameter ψ at tangential vibrations, at a fixed driving velocity v_d and variable amplitude v_a of vibration velocity: (a) longitudinal vibrations, (b) transverse vibrations

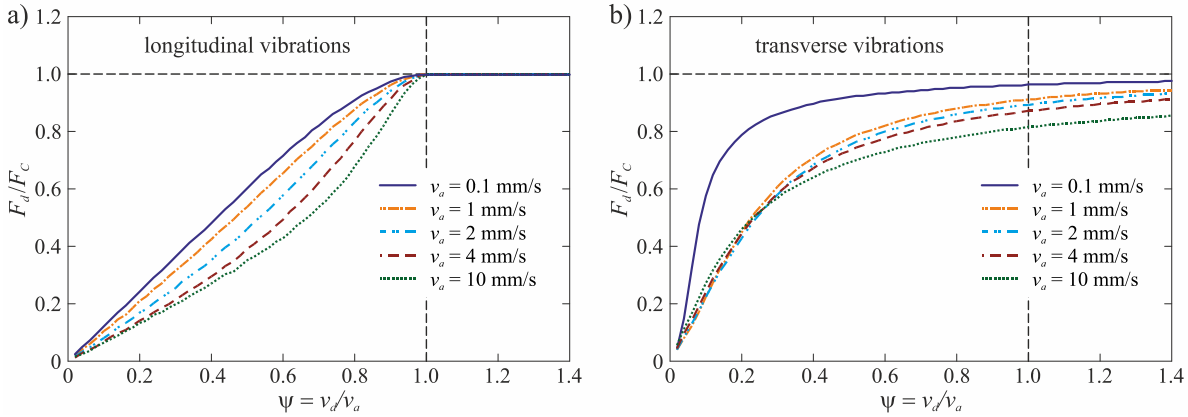

Fig. 6. Profiles of changes in F_d/F_C as a function of parameter ψ at tangential vibrations, at a fixed amplitude v_a of vibration velocity and variable driving velocity v_d: (a) longitudinal vibrations, (b) transverse vibration

Much more complete information about the influence of vibrations on the friction force in sliding motion is provided by collective charts $\mathrm{F_d} = \tilde{\mathrm{F}}_\mathrm{F} = \mathrm{f}(\mathrm{v_a}, \mathrm{v_d})$. For example, in Fig. 7, comparative diagrams are presented regarding the change in the average friction force $\tilde{\mathrm{F}}_\mathrm{F}$ as a function of $\mathrm{v_a}$ and $\mathrm{v_d}$ under longitudinal tangential vibrations and transverse tangential vibrations at the frequency f = 2000 Hz, with surface pressures exerted by the moved body on the support equal to $\mathrm{p_n}$ = 0.022 N/mm2. The presented graphs were generated using computational procedures in which the Dahl model was used to describe the friction force. The comparison of these diagrams shows a clear difference in the effectiveness of reducing the friction force depending on the direction of vibrations. Under transverse vibrations, there are no boundary sliding velocities at which the reduction in friction force would not take place. In longitudinal vibrations, such threshold occurs at $\mathrm{v_a} = \mathrm{v_d}$, but after fulfilling the condition $\mathrm{v_a} > \mathrm{v_d}$, the reduction in the friction force in longitudinal vibrations is clearly greater than that in the case of transverse vibration. In the harmonic motion, described by the following equation:

$$\mathrm{u} = \mathrm{u_0}\sin(\omega\,\mathrm{t}) \tag{13}$$

the amplitude of vibration velocity is expressed by the relationship:

$$\mathrm{v_a} = \mathrm{u_0}\omega = 2\pi\,\mathrm{u_0 f} \tag{14}$$

It is a function of both vibration amplitude $\mathrm{u_0}$ and its frequency f. It can be seen that at a given driving velocity $\mathrm{v_d}$, the condition (12) can be satisfied for different sets of values of parameters $\mathrm{u_0}$ and f, and each of these parameters exerts a nonlinear influence on the level of friction force reduction

Fig. 8 and 9 present examples of simulated results of reduction in friction force in sliding motion on vibrating support as a function of vibration amplitude $\mathrm{u_0}$ at fixed frequency f and as a function of frequency f at fixed amplitude $\mathrm{u_0}$. To facilitate comparison, these graphs were generated for both longitudinal and transverse vibrations of the support.

DOI 10.2478/ama-2024-0013

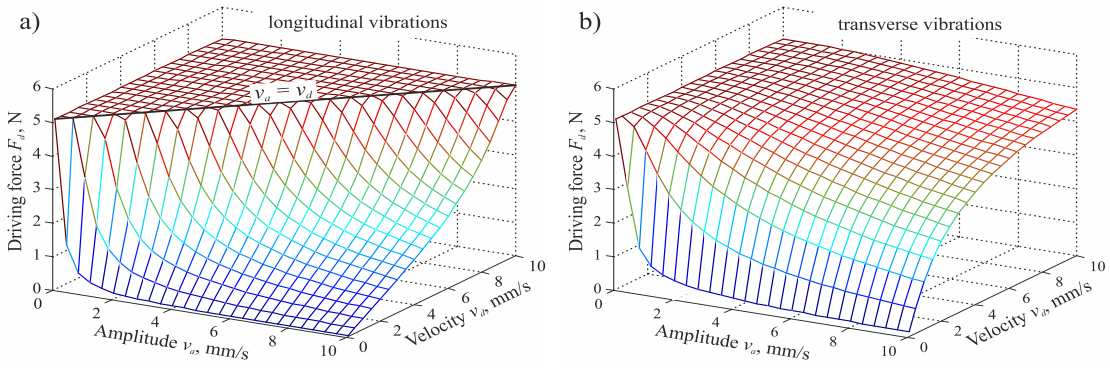

Fig. 7. Dependence of the driving force (average friction force) on the driving velocity v_d and amplitude of vibration velocity v_a: (a) under longitudinal vibrations, (b) under transverse vibrations; f = 2000 Hz, p_n = 0.022 N/mm^2.

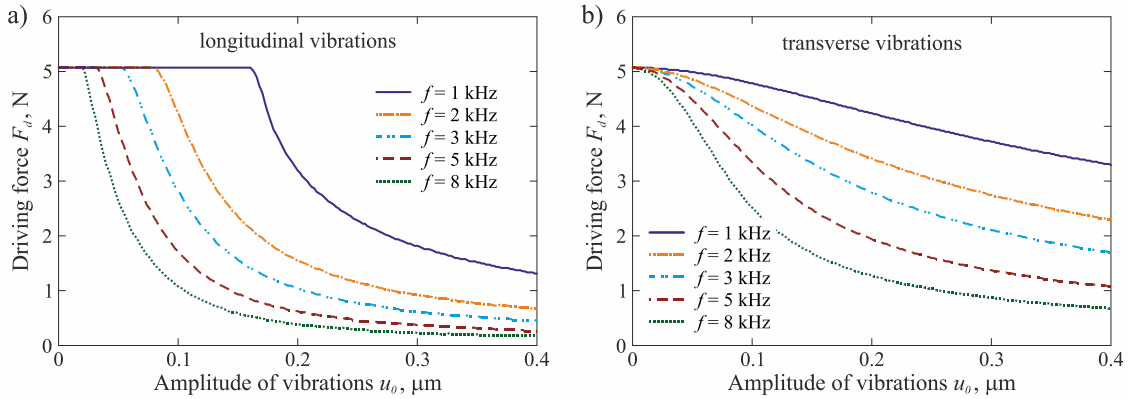

Fig. 8. Change in the driving force F_d as a function of vibration amplitude u_0 at different frequencies f: (a) longitudinal vibrations, (b) transverse vibrations; v_d = 1 mm/s, p_n = 0.022 N/mm^2

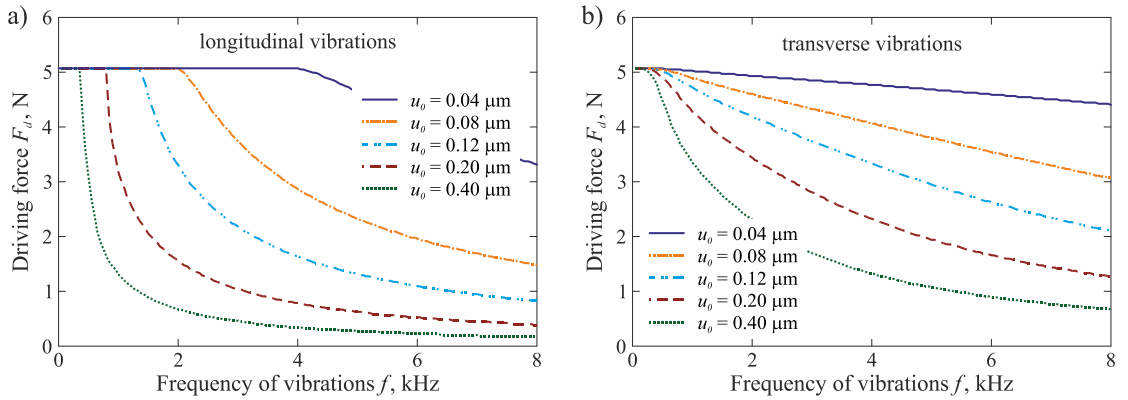

Fig. 9. Change in the driving force F_d as a function of the oscillation frequency f at a given amplitude u_0: (a) longitudinal vibrations, (b) transverse vibrations; v_d = 1 mm/s, p_n = 0.022 N/mm^2

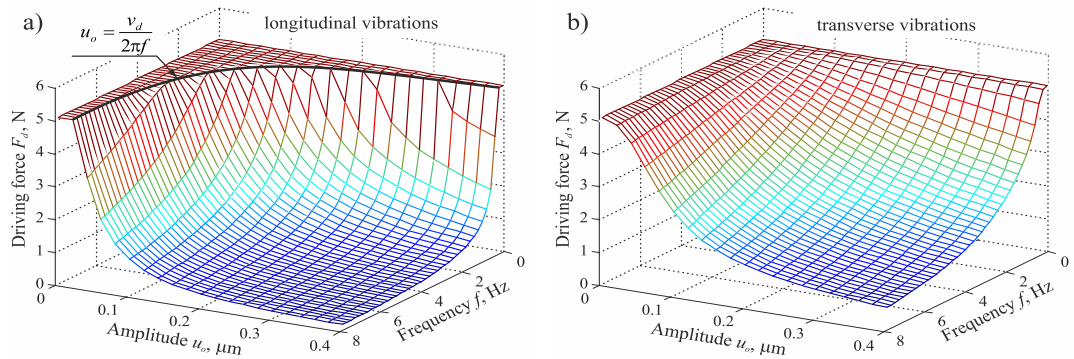

Fig. 10. Change in the driving force (average friction force) in sliding motion depending on the amplitude u_0 and frequency f of vibrations: (a) longitudinal vibrations, (b) transverse vibrations; v_d = 1 mm/s, p_n = 0.022 N/mm2

DOI 10.2478/ama-2024-0013

Based on the set of diagrams shown in Figs. 8 and 9, collective three-dimensional graphs of changes in the average friction force as a function of parameters f and u_0 were generated. They are presented in Fig. 10. It can be seen that with longitudinal vibrations, any reduction in the friction force is possible only after fulfilling the following condition:

$$u_o > \frac{v_d}{2\pi f} \tag{15}$$

which results directly from condition (12) and the relationship (14).

In the case of transverse vibrations, the reduction in the friction force in sliding motion occurs immediately after vibrations are introduced into the contact area of the shifted body and the support, although at low vibration amplitudes and low frequencies, it is at a negligible level.

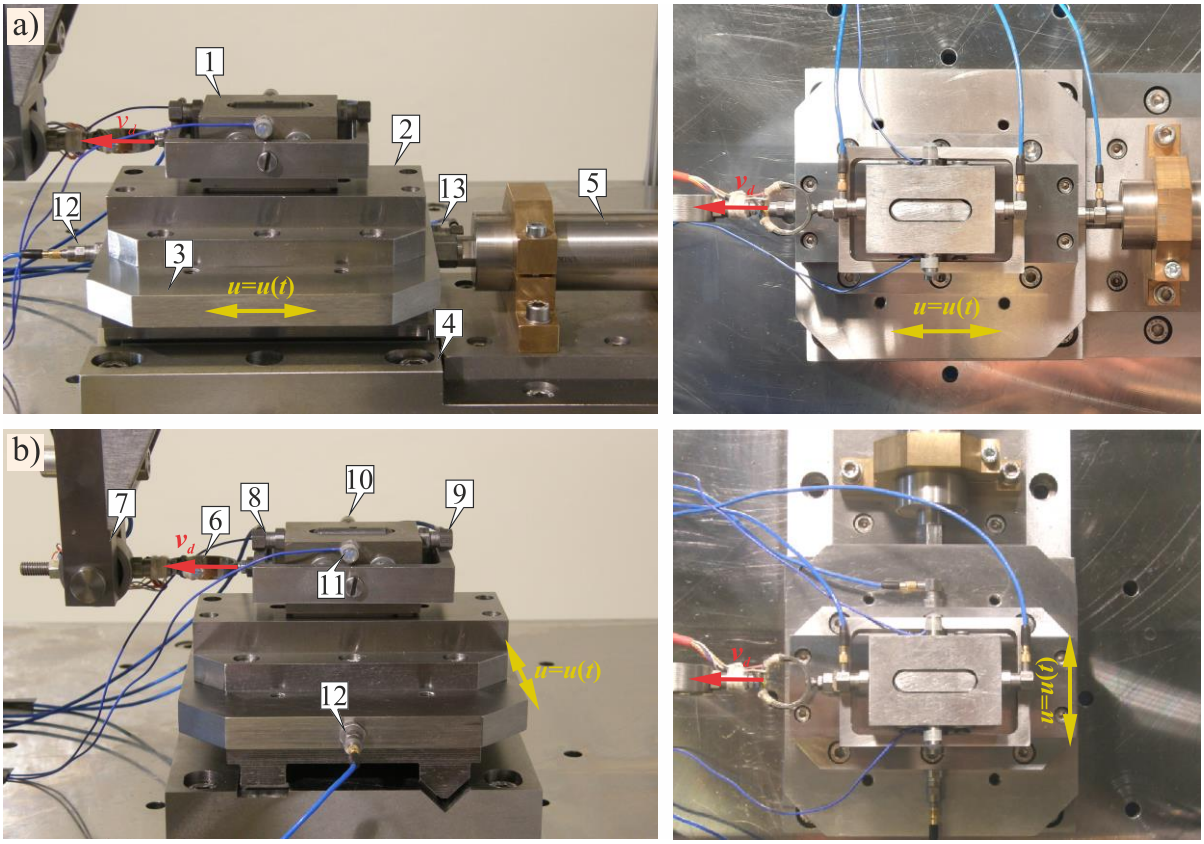

Fig. 11. Mechanical part of the test rig: (a) under longitudinal vibrations, (b) under transverse vibrations; 1 – shifted, upper sample, 2 – bottom sample, 3 – vibrating table, 4 – turn table, 5 – vibration actuator, 6 – force gauge, 7 – driver, 8-13 – accelerometers

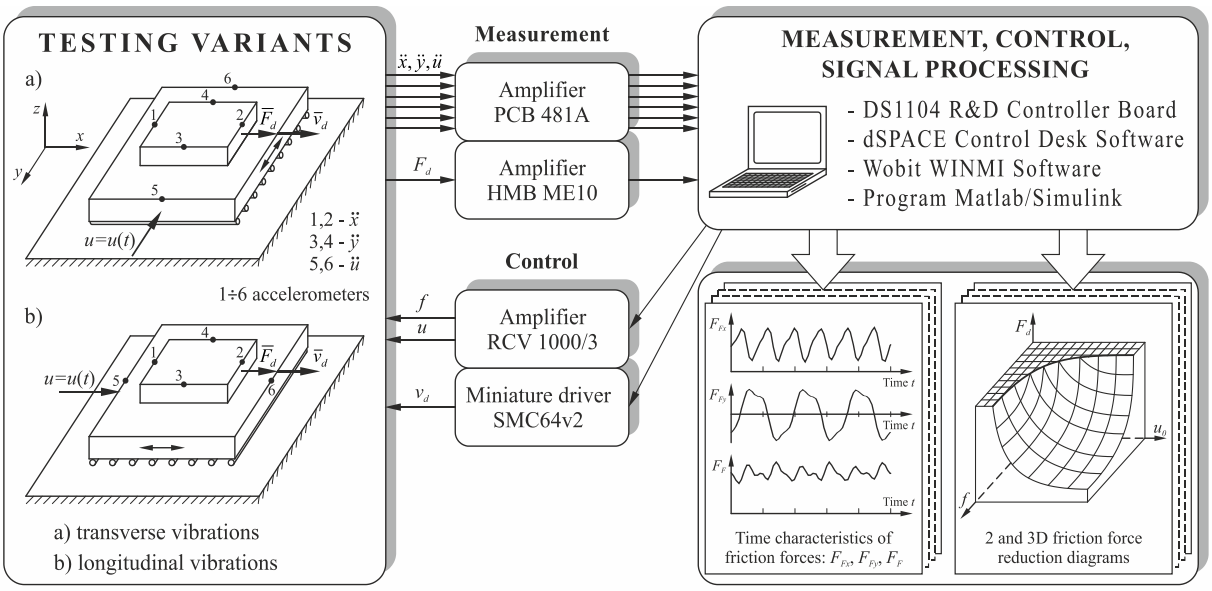

Fig. 12. Block diagram of the measuring, recording and signal processing system

DOI 10.2478/ama-2024-0013

In experiments targeting verification of simulation analyses, the changes in driving force, required to set the body in sliding motion and to sustain this motion, caused by initiating vibrating motion of the support, were measured. The measurements were carried out with longitudinal tangential vibration, that is, consistent with the direction of sliding (Fig. 11a), and with transverse tangential vibrations, that is, perpendicular to this direction (Fig. 11b). They were carried out for two variants of changes in forced vibrations of the support.

In the first variant, the variable parameter was the amplitude u_0 of vibrations at their fixed frequency f, while in the second variant, the variable parameter was the frequency at a fixed amplitude of vibrations. In variant 1, measurements were carried out at a vibration frequency of f = 2000 Hz. The driving velocity was v_d = 1 mm/s, and surface pressure was p_n = 0.022 N/mm^2. In variant 2, it was assumed that the vibration amplitude has the value u_0= 0.2 μm. The frequency was varied in the range from 0 Hz to 5000 Hz. The driving velocity and surface pressures were the same as in variant 1. In each measurement round, the driving force measurement was carried out continuously. Measurements started with motion on an immobilised support, after which it was set in a vibrating motion of gradually increasing frequency (variant 1) or amplitude (variant 2). The last measurement was always carried out after reimmobilising the substrate. Examples of results are presented in Figures 13 and 14.

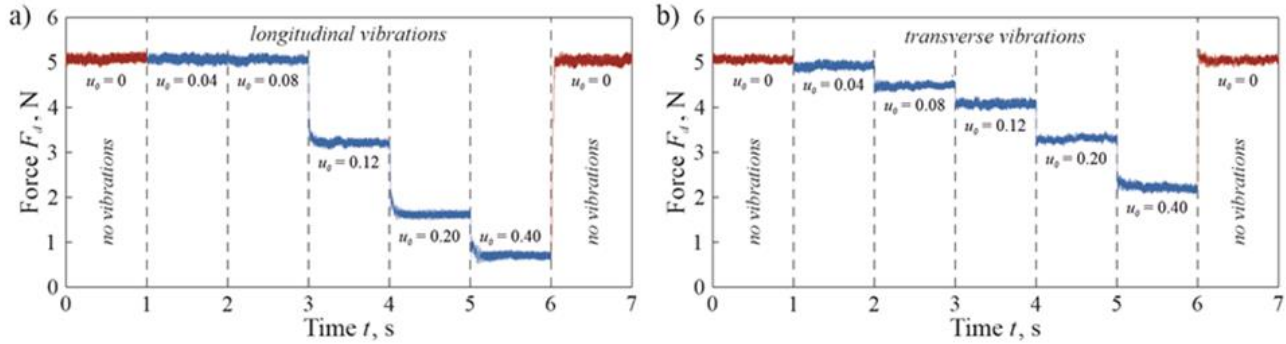

Fig. 13. Change in the driving force F_d in relation to the amplitude u_0 of the support vibrations, at a fixed frequency f: (a) longitudinal vibrations, (b) transverse vibrations; f = 2000 Hz, v_d = 1 mm/s, p_n = 0.022 N/mm^2

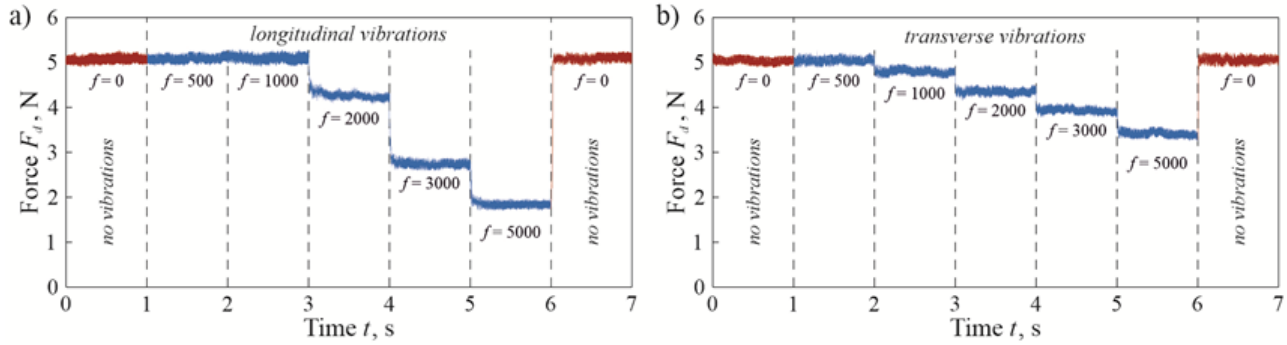

Fig. 14. Change in the driving force F_d in relation to the frequency of vibrations f at their fixed amplitude u_0: (a) longitudinal vibrations, (b) transverse vibrations; u_0 = 0.2 μm, v_d = 1 mm/s, p_n = 0.022 N/mm^2

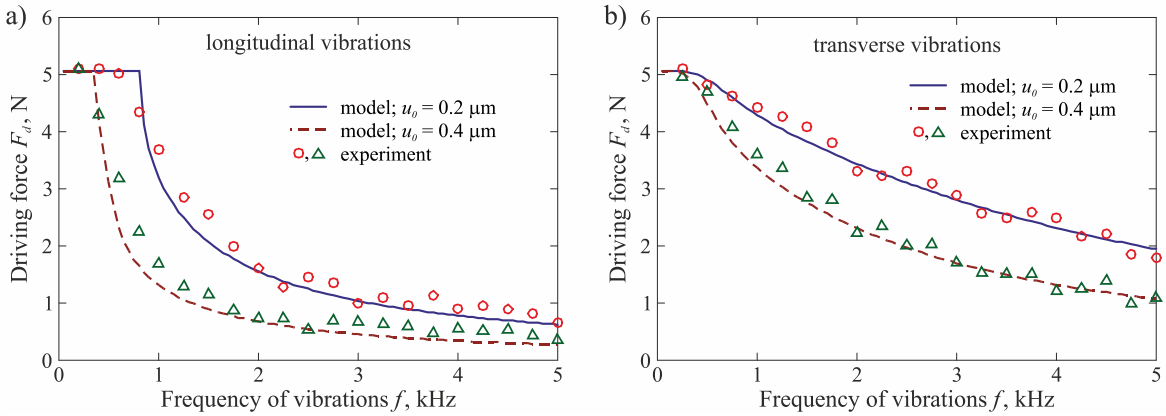

Fig. 15. Comparison of the experimental investigation results and simulating analyses of the friction force reduction depending on the frequency of support vibrations: (a) longitudinal vibrations, (b) transverse vibrations

DOI 10.2478/ama-2024-0013

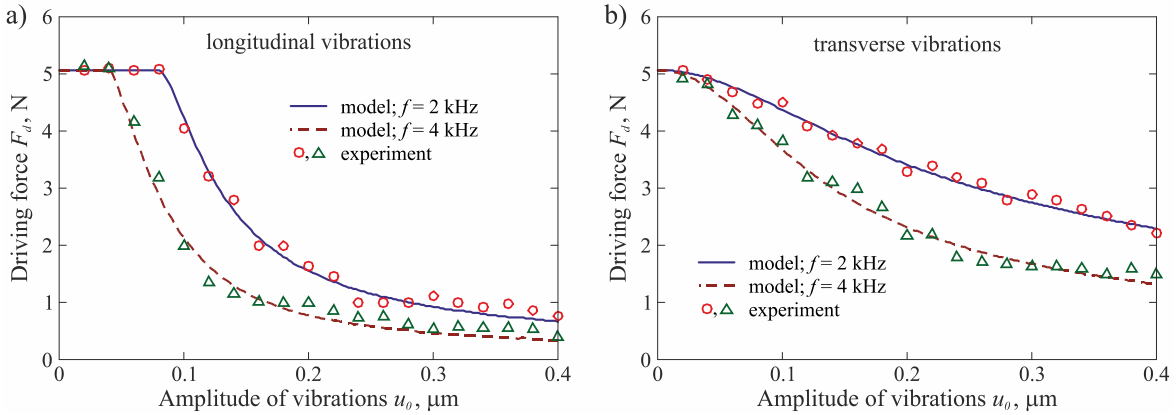

Fig. 16. Comparison of the experimental investigations and simulating analyses of friction force reduction depending on the amplitude of support vibrations: (a) longitudinal vibrations, (b) transverse vibrations

It can be seen from Figures 13 and 14 that in the case of transverse vibrations, the reduction in the friction force occurred immediately after their introduction into the contact area of the shifted body and the support, while in the case of longitudinal vibrations, it occurred only after fulfilling the condition (12). However, after exceeding a threshold value, a further increase in the frequency of vibrations or their amplitude resulted in a much greater reduction in the friction force under longitudinal vibrations.

Figures 15 and 16 present a comparison of the results of simulating computations and experimental investigations. Their excellent conformance is noticeable, which proves the correctness of the developed models and numerical computational procedures.

4. SUMMARY

Very good agreement between the outcome of simulating analyses and experimental investigations proves that the computational models used in numerical analyses are (i) developed correctly and (ii) accurately reflect the actual changes in the friction force occurring in sliding motion upon exerting vibrational movements to the support over which such sliding motion is performed. This suggests that these models can be utilised for controlling the friction force in sliding motion through an appropriate selection of vibration parameters u_0 and f of the support, on which such motion takes place.

Experimental investigations and simulating analyses have demonstrated that under longitudinal vibrations, when the threshold value of amplitude v_a of vibration velocity ($v_a = v_d$) is exceeded, the level of friction force reduction in sliding motion increases with increasing vibration amplitude u_0 or their frequency f, to much greater extent than under transverse vibrations. However, up to this threshold value, longitudinal vibrations, in contrast to transverse vibrations, have no effect on the level of the friction force.

REFERENCES

1. Czon Y, Su H, Qian N, He J, Gu J, Xu J, et al. Ultrasonic vibration assisted grinding of silicone carbide ceramics based on actual amplitude measurement: grinding force and surface quality. Ceramics International. 2021;47(11): 15433–15441. https://doi.org/10.1016/j.ceramint.2021.02.109
2. Gao G, Xia Z, Su T, Xiang D, Zhao B. Cutting force model of longitudinal–torsional ultrasonic-assisted milling Ti-6Al-4V based in tool flank wear. Journal of Materials Processing Technology. 2021; 291:117042. https://doi.org/10.1016/j.jmatprotec.2021.117042
3. Jamshidi H, Nategh MJ. Theoretical and experimental investigation of the frictional behavior of the tool-chip interface in ultrasonic-vibration assisted turning. International Journal of Machine Tools and Manufacture. 2013;65:1–7. https://doi.org/10.1016/j.ijmachtools.2012.09.004
4. Khajehzadeh M, Bootaripour O, Razfar MR. Finite element simulation and experimental investigation of residual stresses in ultrasonic assisted turning. Ultrasonics. 2020;108:106208. https://doi.org/10.1016/j.ultras.2020.106208
5. Li D, Tang J, Czen H, Shao W. Study on grinding force model in ultrasonic vibration-assisted grinding alloy structural steel. The International Journal of Advanced Manufacturing Technology. 2019; 101:1467–1479. https://doi.org/10.1007/s00170-018-2929-2
6. Liu Y, Geng D, Zhou Z, Jiang X, Zhang D. A study of on strengthening and machining integrated ultrasonic peening drilling of Ti-6Al-4V. Materials & Design. 2021; 212:110238. https://doi.org/10.1016/j.matdes.2021.110238
7. Ning F, Cong W. Ultrasonic vibration-assisted (UV-A) manufacturing processes: state of art and future perspectives. Journal of Manufacturing Processes. 2020;51:174–190. https://doi.org/10.1016/j.jmapro.2020.01.028
8. Skeleton RC. Effect of ultrasonic vibration on the turning process. International Journal of Machine Tool Design and Research. 1969;9(4):363–374. https://doi.org/10.1016/0020-7357(69)90020-1
9. Wang H, Pei ZJ, Cong W. A mechanistic cutting force model based on ductile and brittle fracture material removal modes for edge surface grinding of CFRP composites using rotary ultrasonic machining. International Journal of Mechanical Sciences. 2020;176:105551. https://doi.org/10.1016/j.ijmecsci.2020.105551
10. Wang J, Zhang J, Feng P, Guo P. Experimental and theoretical investigation of critical cutting force in rotary ultrasonic drilling of brittle materials and composites. International Journal of Mechanical Sciences. 2018;135:555–564. https://doi.org/10.1016/j.ijmecsci.2017.11.042
11. Verma GC, Pandey PM. Machining forces in ultrasonic vibration assisted end milling. Ultrasonics. 2019;94:350–363. https://doi.org/10.1016/j.ultras.2018.07.004
12. Aarsnes UJ, Di Meglio F, Shor RJ. Avoiding stick slip vibration in drilling through startup trajectory design. Journal of Process Control. 2018;70:24–35. https://doi.org/10.1016/j.jprocont.2018.07.019
13. Barakat ER, Miska S, Mengjlao Y, Simonescu PA, Takch N. The effect of hydraulic vibrations on initiation of buckling and axial force transfer for helically buckled pipes at simulated horizontal wellbore conditions. Proc SPE/IADC Drill Conf Exhib, Amsterdam, The Netherlands, February 2007.

14. Gee R, Hanley C, Hussain R, Cannel L, Martinez J. Axial oscillations tools vs. lateral vibration tools for friction reduction what's the best way to shake the pipe. London: Society of Petroleum Engineers, March 2015.
15. Long Y, Wang X, Wang P, Zhang F. A method of reducing friction and improving the penetration rate by safely vibrating the drill-string at surface. Processes. 2023; 11(4):1242. https://doi.org/10.3390/pr11041242
16. Maidla E, Haci M, Jones S, Cluchy M, Alexander M, Warren T. Field proof of the new sliding technology for directionnal drilling. Proceedings of the SPE/IADC Drilling Conference, Amsterdam, The Netherlands, February 2005.
17. Roper NF, Dellinger TB. Reduction of frictional coefficient in borehole by use of vibration. 1983: US 4384625 1983-05-24.
18. Skyles LP, Amiraslani YA, Wilhoit JE. Converting static friction to kinetic friction to drill further and faster in directional holes. Proceedings of the IDAC/SPE Drilling Conference and Exhibition. San Diego CA, USA, 6–8 March 2012.
19. Qiu H, Yang J, Butt S. Investigation on bit stick-slip vibration with random friction coefficients. Journal of Petroleum Science and Engineering. 2018;164:127–139. https://doi.org/10.1016/j.petrol.2018.01.037
20. Zhu X, Tang L, Yang Q. A literature review of approaches for stick-slip vibration suppression in oil well drill-string. Advances in Mechanical Engineering. 2014;6:967952. https://doi.org/10.1155/2014/967952
21. Leus M, Gutowski P. The analysis of longitudinal contact vibration effect on friction force using Coulomb and Dahl models. Journal of Theoretical and Applied Mechanics. 2008; 46(1):171–84 [in Polish].
22. Gutowski P, Leus M. The effect of longitudinal tangential vibrations on friction and driving forces in sliding motion. Tribology International. 2012; 55: 108–118. https://doi.org/10.1016/j.triboint.2012.05.023.
23. Dahl PR. A solid friction model. Technical Report TOR-158(3107-18), The Aerospace Corporation, El Segundo, CA, 1968.
24. Dahl PR. Solid friction damping of mechanical vibrations. AIAA Journal. 1976;14(12):1675–1682. https://doi.org/10.2514/3.61511.
25. Dupont P, Armstrong B, Hayward V. Elasto-plastic friction model: contact compliance and stiction. Proceedings of the American Control Conference, Chicago, Illinois 2000:1072–1077. https://doi.org/10.1109/ACC.2000.876665.
26. Dupont P, Hayward V, Armstrong B, Altpeter F. Single state elasto-plastic friction models. IEEE Transactions on Automatic Control. 2002; 47(5):787-792. https://doi.org/10.1109/TAC.2002.1000274.
27. Storck H, Littmann W, Wallaschek J, Mracek M. The effect of friction reduction in presence of ultrasonic vibrations and its relevance to traveling wave ultrasonic motors. Ultrasonic. 2002;40:379–383. http://dx.doi.org/10.1016/S0041-624X(02)00126-9.
28. Tsai CC, Tseng CH. The effect of friction reduction in presence of in-plane vibrations. Archive of Applied Mechanics. 2006;75:164–76. https://doi.org/10.1007/s00419-005-0427-0.
29. Gutowski P, Leus M. Computational model for friction force estimation in sliding motion at transverse tangential vibrations of elastic contact support. Tribology International. 2015;90:455–462. https://doi.org/10.1016/j.triboint.2015.04.044.
30. Gutowski P, Leus M. Computational model of friction force reduction at arbitrary direction of tangential vibrations and its experimental verification. Tribology International. 2020;143:106065. https://doi.org/10.1016/j.triboint.2019.106065.
31. Godfrey D. Vibration reduces metal to metal contact causes an apparent reduction in friction. ASLE Transactions. 1967;10:183–192. https://doi.org/10.1080/05698196708972178.
32. Hess DP, Soom A. Normal vibrations and friction under harmonic loads: part I – Hertzian contacts. Journal of Tribology. 1971;113:80–86. https://doi.org/10.1115/1.2920607.
33. Tolstoi DM, Borisova GA, Grigorova SR. Friction regulation by perpendicular oscillation. Soviet Physics – Doklad. 1973;17(9):907– 909.
34. Canudas de Wit C, Olsson H, Astrom KJ, Lischynsky P. A new model for control of systems with friction. IEEE Transactions of Automatic Control. 1995;40(3):419-425. https://doi.org/10.1109/9.376053.
35. Olsson H. Control systems with friction. Lund 1996.
36. Bliman PA. Mathematical study of the Dahl's friction model. European Journal of Mechanics, A/Solids. 1992;11(66):835–848.

Mariusz Leus: https://orcid.org/0000-0002-1073-1734

Paweł Gutowski: https://orcid.org/0000-0002-0618-2357